J Mater Sci (2009) 44:3643–3651
DOI 10.1007/s10853-009-3481-0

Influence of carbon fibre treatment and filler addition on porosity and structure change of carbon fibres reinforced phenolic matrix composites during carbonization

Pierre Baudry · Marie-Anne Dourges · René Pailler

Received: 4 November 2008 / Accepted: 9 April 2009 / Published online: 5 May 2009

Abstract The transformation during pyrolysis of ex-cellulose carbon fibres/phenolic matrix 2D composites is investigated. The amount and the dimensions of pores and micro-cracks created after heat treatment are characterized and described from 600 °C (resin pyrolysed matrix) to 1,000 °C (carbonized matrix). Characterization of samples was performed using mercury intrusion porosimetry at different stages of thermal treatment. Three different composites were prepared in order to study the influence of fibre surface properties and the role of carbon filler addition in matrix, on the porosity emergence. Inter-laminar shear strengths of these materials were recorded. On the investigated materials, the lowest fibre/matrix bonding is found to preserve material cohesion by promoting interfacial debonding and thus limiting consequences of shrinkage during matrix carbonization.

Introduction

Carbon/carbon composites (C/C) are the most suitable thermo-structural material for certain aeronautics and aerospace applications, considering their mechanical performances at high temperatures. Among the possibilities of fabrication, one process consists in polymer impregnation of fibre preform with suitable precursor, to produce Carbon/Resin (C/R) material and pyrolysis to obtain a C/C composite. Thermosetting resins are commonly used as matrix precursor due to the good flexibility of processing. Phenolic resins are chosen because of their high carbon yield after pyrolysis. The matrix material produced by this way is characterized by low-mechanical properties (when compared with chemical vapour deposition- derived carbon), an isotropic structure and a nanoporous microstructure. The pyrolysis of C/R results in a complex combination of thermo-physical and chemical phenomena. A porous composite is obtained after a first impregnation/pyrolysis process. The internal stress generated in composites could be due to phenomena identified as: (i) fibre and matrix differential thermal expansion, (ii) resin dilatation during the first step of transformation (drying) and resin shrinkage during matrix carbonization. This is connected to the development of porosity and cracks in the composite, with consequences in releasing interfacial stresses by debonding and creating exit path for gas products. Controlling porosity and thus gas permeation during carbonization is thought to lead to control residual stresses and enhance C/C mechanical properties in the final material.

The chemical pyrolysis of the resin has been extensively investigated and mechanisms of carbonization were proposed [1]. The extent and consequences of matrix shrinkage have also been widely studied, modelled and reviewed [2, 3]. The stress state variations within C/R composites during the carbonization of the phenolic matrix (<1,000 °C) have been found to influence the residual carbon ability to develop further organization [4–6]. It has been proposed [7] that the matrix structure in C/C depends on the strain state created through matrix restrained shrinkage at the fibre/matrix interface. It implies that the composite structure could depend on interfacial bonding [8] during carbonization. This parameter variation during composite pyrolysis is still uncertain. The initial carbon fibre/phenolic matrix bonding is known to be of chemical type [9]. Recent

P. Baudry · M.-A. Dourges (✉) · R. Pailler
Laboratoire des Composites Thermo-Structuraux, UMR 5801(CNRS-SAFRAN-CEA-UB1), Université Bordeaux1, 3 Allée de la Boétie, 33600 Pessac, France
e-mail: dourges@lcts.u-bordeaux1.fr

published works [10] on model unidirectional C/R composites proposed that this bonding changes from chemical to mechanical type during pyrolysis, involving fibres surface morphology. A strong initial fibre/matrix (f/m) bonding would promote directional shrinkage onto the fibres. It would cause strong f/m mechanical interactions at a temperature at which fibre surface functions have been removed. The strain state created during this matrix shrinkage step is restrained by fibres architecture but may be strong enough to cause matrix failure and/or fibre matrix debonding, and results in the development of a voids and cracks network in 2D-composites. This porosity has been described in pyrolysed cellulosic-based carbon C/R 2D-composites using image analysis [11]. The extent of the different listed porosity types (namely co-planar cracks, bundle cracks, inter-fibre pores and inter-fibre cracks) was evaluated on material cross-sections. Porosity could not be clearly related to carbon-fibres properties or precursor. The porosity network in 2D-composite is supposed to depend more on processing techniques and reinforcement architecture than on fibre properties.

Another recent publication presents a work describing crack development during pyrolysis of carbon fibre reinforced polymer [12] (tenax HTA fibres/highly aromatic resin). Authors utilize dilatometer analysis, thermo-microscopy and acoustic emission to study the mechanisms of cracking. The phenomenon is characterized by successive emergence of several types of cracks; micro-cracks due to fibre–matrix debonding at microscopic scale, transversal cracks and partial delamination at mesoscopic scale.

The mechanical behaviour of PAN-based 2D-C/R during pyrolysis has been reported [13, 14]. Strong initial f/m bonding confers a brittle behaviour to corresponding C/C, whereas interfaces in weak-bonded C/R tend to debond and to annihilate load transfer in resulting C/C. The crack network and/or matrix structure also limit the composites cohesion and inter-laminar shear strength. The dispersion of carbon filler is an alternative way to modify matrix properties [15] and reduce resin content. Adduct of filler can also prevent f/m interfacial stress either by promoting filler/matrix debonding and cracks deviation (weak filler/matrix bonding) or by concentrating resin shrinkage onto filler particles (strong filler/matrix bonding).

Anticipation of C/R-derived C/C composites properties requires understanding f/m bonding change during pyrolysis, and its influence on material porosity and matrix structure development. The present study deals with the comprehension of the link between interfacial phenomena at polymer stage and matrix structural characteristic along pyrolysis in real-sized phenolic matrix composites reinforced with 2D cellulosic-based carbon preform. Mercury intrusion porosimetry and microscopic observations are used to investigate the porosity network and the carbonaceous matrix microstructure during four or five stages of carbonization up to 1,000 °C for the three different composites, and to evaluate porosity influence on materials properties.

Experimental

Material

Cellulose-based carbon fibres (further referred to as F) were treated to modify their surface properties (fibres referred to as F_t). Eight-harness satin-weave fabrics of these two types of fibres were impregnated with a phenolic resin, with or without carbon filler. The resulting prepregs were cut, piled up and moulded under pressure to obtain $100 \times 160 \times 60\ mm^3$ specimen. All treatments were made by SPS (Snecma Propulsion Solid-SAFRAN group) and the details of which are confidential. These materials are presented in Table 1.

Resin matrices were pre-cured and cured up to 180 °C following a classical polymerization cycle. Composite samples were then pyrolysed in an inert atmosphere (pure N_2) at different temperatures up to carbonization (1,000 °C) with a 100 °C/min heating rate. This unusually high heating rate is supposed to accentuate the micro-cracking phenomena during heat treatment [16].

Characterization

Surface properties

Fibres surface properties were investigated using X-ray photoelectron spectroscopy (XPS, VG220iXL) to measure their oxygen content. Atomic force microscopy (AFM) was performed using a Nanoscope III (Digital Instrument) to evaluate the fibres surface roughness. The raw data supplied by AFM recording was processed to obtain the 'average roughness' value R_a with a method described elsewhere [17].

Density and open porosity

Material densities (called true densities) were measured by helium pycnometry (Micromeritics AccuPyc 1330). Open

Table 1 Elaborated composites references and compositions

Reference	Fibre type	Matrix	Filler
F/P	F	Phenolic	None
F/P_f	F	Phenolic	Carbon
F_t/P_f	F_t	Phenolic	Carbon

porosity was then deduced from geometrical density measurements. Porosity was also characterized by mercury intrusion porosimetry (Micromeritics Autopores IV).

Structure and morphology

The specific surfaces of the composite constituents were determined conventionally with CO_2 or N_2 gas adsorption (Micromeritics ASAP2010) using BET theory. Composites treated at different temperatures were investigated by optical microscopy (Nikon ME600) after classical polishing way of 10×10 mm^2 surface samples. Interfacial structures were observed using transmitted electron microscopy (TEM, Phillips CM30ST) in cured composites.

Mechanical properties

The composite cohesion was tested at different steps of the pyrolysis by measuring inter-laminar shear strength (ILSS) of samples submitted to double-notched compression (DNC) test. Samples dimensions are reported in Fig. 1.

The shear tested direction is along the fibres reinforced direction, and the specimens are prevented from buckling by an adapted tool [18]. Four to six samples are tested in each case.

Results and discussion

Material composition and characteristics

Data collected on investigated carbon fibres and fillers are summarized in Table 2.

The morphology of the two investigated fibres is very close. At a 100 nm scale, the average roughness is low for both fibres. The specific area has been drastically reduced by the fibre treatment. From the lower F_t density, it can be inferred that the treatment experienced by this fibre results

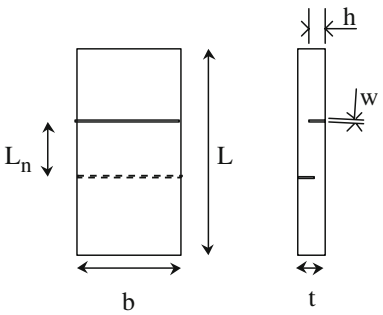

Fig. 1 Double-notched compression specimen dimensions: $L = 30$, $b = 15$, $L_n = 8$, $t = 4$, $W = 0.3$, $h = 2.3$ in mm

Table 2 Fibres and fillers properties

	F fibre	F_t fibre
Fibre section area (μm^2)	50 ± 5	50 ± 5
He apparent density (g cm^{-3})	1.88 ± 0.01	1.61 ± 0.01
Specific area (m^2/g)	343 ± 5 (CO_2)	1.73 ± 0.1 (N_2)
Surface pH[a]	9	7
Surface atomic composition (%)	C (82.3%)	C (87.3%)
	O (14.4%)	O (10.7%)
	Si (3.3%)	Na (2.0%)
Surface O/C elemental ratio	0.17	0.12
Roughness 100 × 100 nm^2 (nm)	0.8 ± 0.1	1.1 ± 0.1
		Carbon filler
He apparent density (g/cm^3)		1.73 ± 0.01
Specific area (m^2/g)		12.8 ± 0.4

[a] Data from material supplier

Table 3 Materials volume composition

Material	Fibre volume fraction	Filler volume fraction	Open porosity fraction	Matrix volume fraction
F/*P*	0.51 ± 0.03	0	0.03 ± 0.01	0.45 ± 0.04
F/P_f	0.46 ± 0.03	0.10	≤0.01	0.43 ± 0.03
F_t/P_f	0.53 ± 0.03	0.08	0.01 ± 0.01	0.38 ± 0.03

in closing the surface pores present on the *F* fibre. Moreover, the surface oxygen content is lower for the F_t than for the *F*. For these two reasons, the F_t fibre ability to interact with a phenolic matrix is suspected to be lower than for the *F* fibre.

Table 3 shows the cured C/R material volumes repartition as deduced from material supplier data and He pycnometry data assuming a negligible closed porosity and a constant matrix density of 1.28 g/cm^3.

In order to observe fibre/matrix interface in C/R state, investigations were carried out using transmission electron microscopy. Green F/P_f and F_t/P_f composite samples are prepared by classical techniques with final ion-beam thinning. The cohesion of intra-bundles zones remains high enough to allow performing transmission electronic microscopy. Interfaces are bonded in as-cured F/P_f composite and debonded in as-cured F_t/P_f composite as it was observed on TEM micrographs (Fig. 2). This debonding may be due to differential thermal expansion during cooling or possibly to the preparation stresses. In both cases, itcorroborates the hypothesis of a lower adhesion of the F_t fibre to the matrix when compared with *F*/matrix bonding.

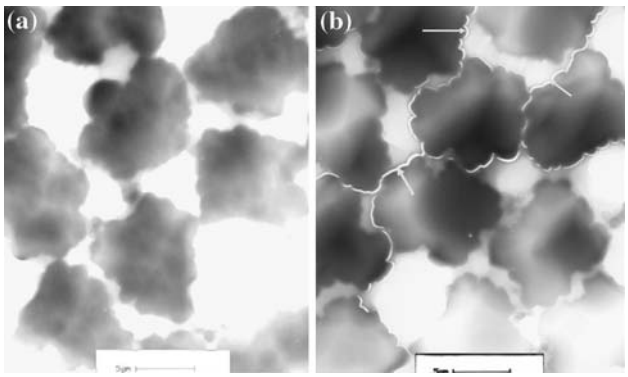

Fig. 2 **a** Cohesive fibre/matrix interfaces in as cured F/P_f and non-cohesive interfaces in as cured F_t/P_f composite (**b**)

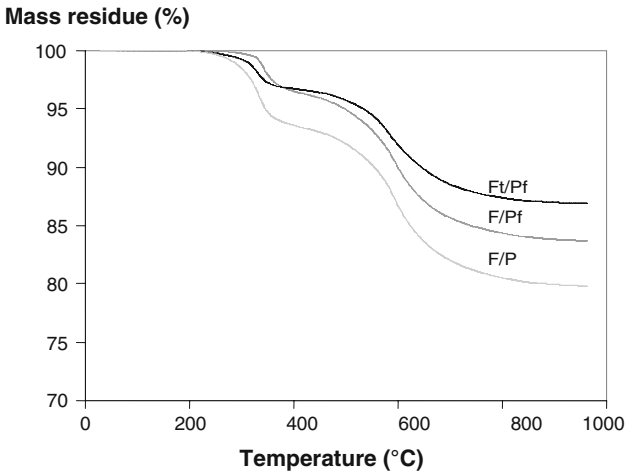

Fig. 3 Examples of *C/phenolic matrix composites* TGA curves

Composites pyrolysis

C/R composites were analyzed by TGA with a 100 °C/min heating rate under N_2 flow (Fig. 3). The general variation of the composites mass loss curves between 20 and 1,000 °C exhibits two major stages.

The first mass loss centred on 300 °C is mainly due to the evolution of free water in the samples [19], and to the elimination of residual solvent in resin. The matrix, filler and fibre different contents in these composites could explain the different values of this first mass loss, with a more important evolution of water in the composite without filler and with higher porosity.

The second mass loss occurs between 400 and 800 °C for the three samples with the inflexion point centered at 590 ± 5 °C. As the fibres and filler mass remain constant because of their higher processing temperature, the mass loss is ascribed to the phenolic resin chemical transformation. Profile of weight loss is close to the one reported in former studies [1] during the pyrolysis of C/R composites, with a shift of starting reaction temperature due to the relatively high heating rate of 100 °C/min. The values of the second mass loss depend on initial composition of the samples.

Variation of density and porosity with treatment

Variations of composite densities during pyrolysis are shown in Fig. 4. The values of geometrical densities decrease from 1.42 to about 1.2 g/cm^3 and are almost independent of the composites nature. This decrease is a consequence of the ~2% composite expansion measured on all samples through the thickness. This change is due to inter-laminar cracking and delaminating process during pyrolysis that will be described further. The true density (obtained using helium pycnometry method) increases with temperature treatment, as a consequence of resin carbonization and shrinkage. The initial and final values are the same for the three composites, but the variation during resin pyrolysis are different. The F/P and F/P_f composites reach their maximal densities, respectively, at 600 and 800 °C, whereas the F_t/P_f true density increases linearly all along the pyrolysis. As the differences in materials geometrical densities remain low until 1,000 °C, it means that the open porosity volume is created before 600 °C for F/P, before 800 °C for F/P_f, and increases during the whole treatment for F_t/P_f (Fig. 5).

Mercury intrusion porosimetry (MIP) is performed on investigated materials and the curves of the open porosity volume corresponding to equivalent cylinder-shaped pores diameter distribution are detailed in Fig. 6.

The processing of these data in order to define material apparent pore size distribution was discussed in former published works [20]. The Washburn equation is used to

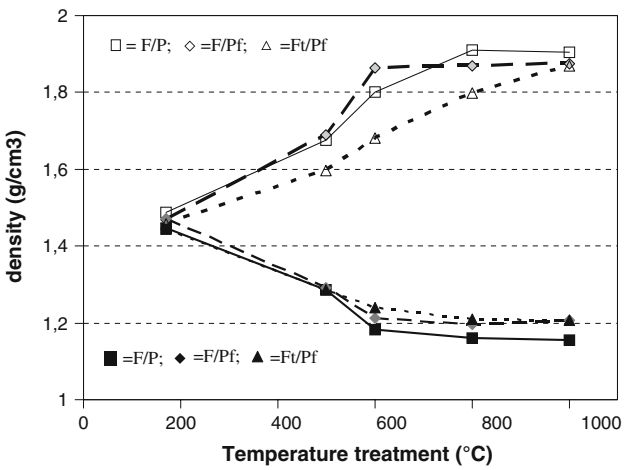

Fig. 4 True density (*open symbols*) from He pycnometry experiment and geometrical density (*filled symbols*) of heat treated composites

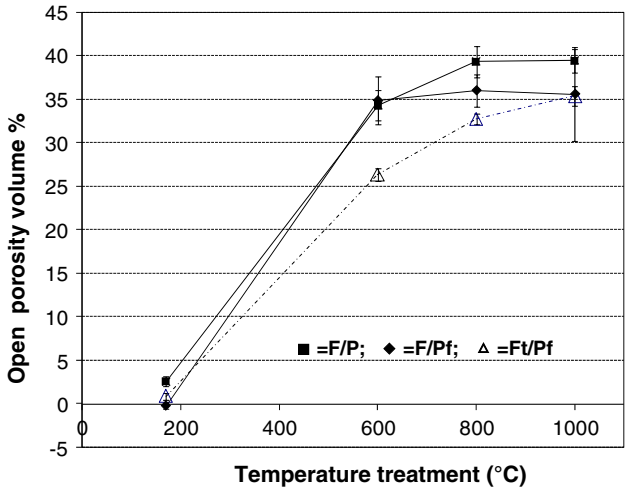

Fig. 5 Open porosity of heat treated composites

correlate the pore radius r to given mercury intrusion pressure P:

$$P = -2v\frac{\cos\theta}{r}$$

where v is the surface tension of mercury and θ the material/mercury contact angle (155°). This equation assumes an unconnected cylindrical shape for the pores that is rarely found in real materials. Connected pores or fractures with various shape and size will obviously not be precisely measured by this method, especially when large pores are connected through small ones: that causes the whole porosity to be attributed to a small size pore population. The reproducibility of this technique has also been reported to be high, and the compressibility effect to be of small influence [21]. In materials with extended and large size porosity networks like pyrolysed carbon/phenolic composites, the pore size distribution is obtained with a good accuracy when compared with SEM analyses [22]. The tortuosity effect described above is in this case by-passed during intrusion by the large fractures network. The reproducibility of the method is actually found to be good on these highly cracked composites. This technique does not take into account the pores sizes under 0.01 μm. The volumes of the pores with equivalent diameter under 10 nm are calculated by difference between the true density and density measured with mercury intrusion method.

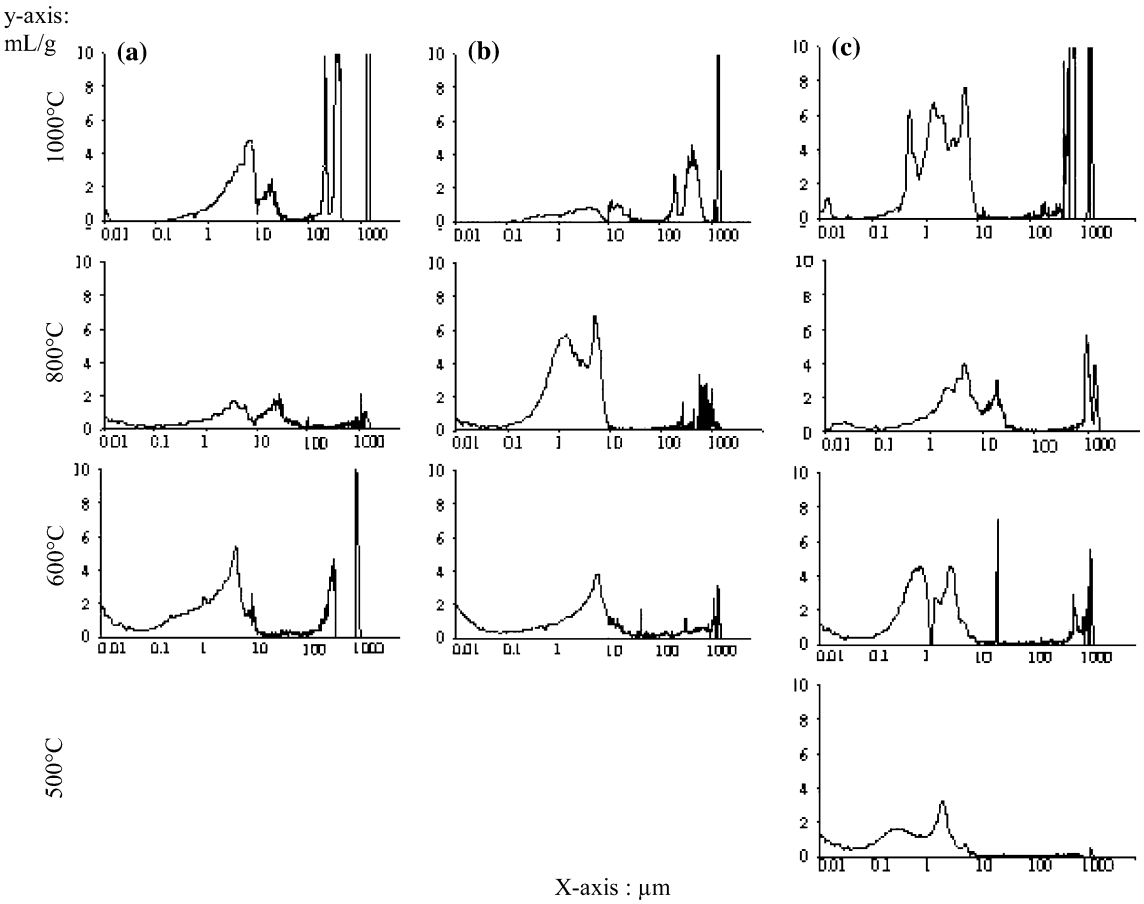

Fig. 6 Porosity volume (mL/g) versus apparent pore size distribution (μm) for the **a** *F*/*P*, **b** *F*/PF and **c** F_t/P_f composites heat treated at 500, 600, 800 and 1,000 °C

In the following, closed porosity will be assumed to be negligible compared with open porosity. Perpendicular-to-reinforcement-plane cross-sections along woven axes are found to be equivalent by optical microscopy. Fibres extraction has been noted to be higher with F_t/P_f samples and has to be taken into account for microscopic analysis.

The MIP curves show porosity populations whose limit sizes are listed in Fig. 7. An independent study of micrographs allows defining cracks types. The dimension of these cracks types on micrographs are found to correspond with porosity diameter recorded by MIP. The volumes corresponding to each pore population are indicated in Fig. 8. These volumes are in good agreement with values estimated by 2D image analysis on materials cross sections.

The initial porosities of the composites are relatively low (Fig. 9) and consist in small-sized pores, which are thought to be due to impregnation defects and fibre micro pores.

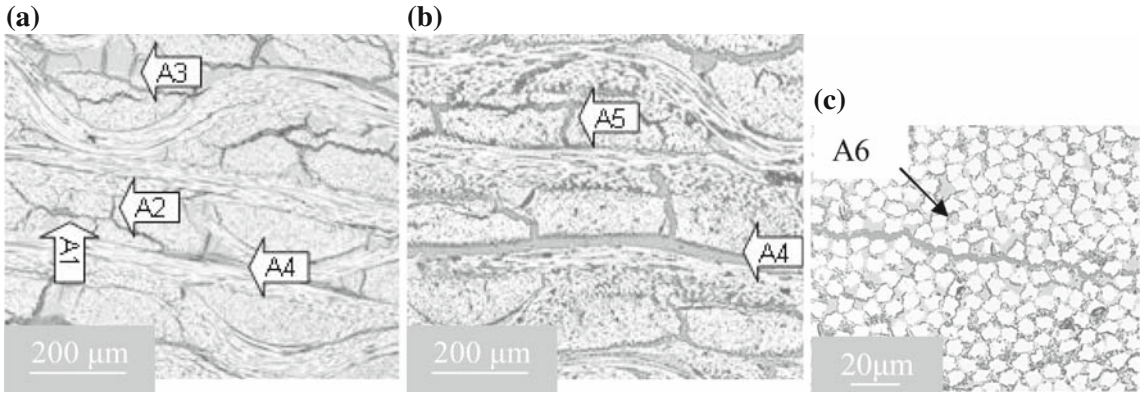

(d)

	Porosity class	Characteristic size
A1	*Intra-bundle longitudinal cracks*	5 - 50µm
A2	*Intra-bundle transverse cracks*	
A3	*Intra-matrix transverse cracks*	10 - 50µm
A4	*Inter-laminar cracks and delaminating*	> 50 µm
A5	*Inter-bundle cracks*	10 – 50 µm
A6	Fibre/matrix debonding	0.01 – 5 µm

Fig. 7 Optical micrographs of **a** F/P, **b** F/P_f, composites heat treated at 600 °C (100 °C/min). **c** Enlargement showing fibre/matrix debonding on F_t/P_f material. The table describes the corresponding porosity classes

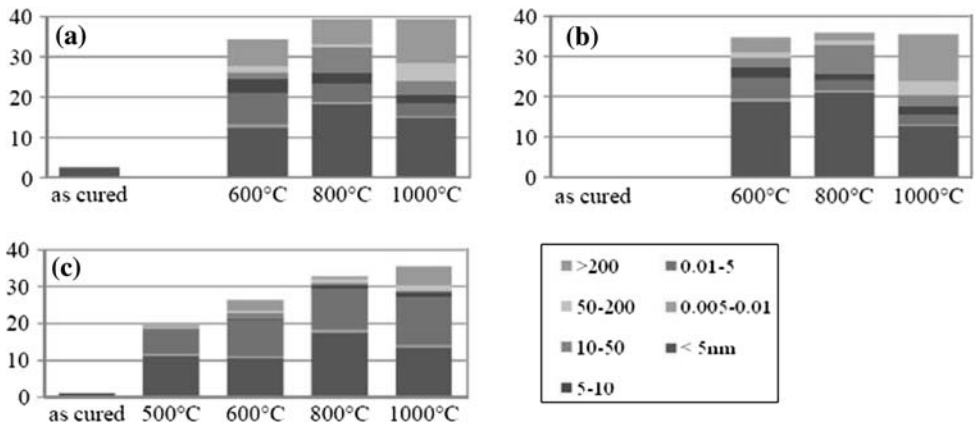

Fig. 8 Volumes distribution (%) of pores apparent diameter (µm) in heat treated composites for F/P (**a**), F/P_f (**b**) and F_t/P_f (**c**)

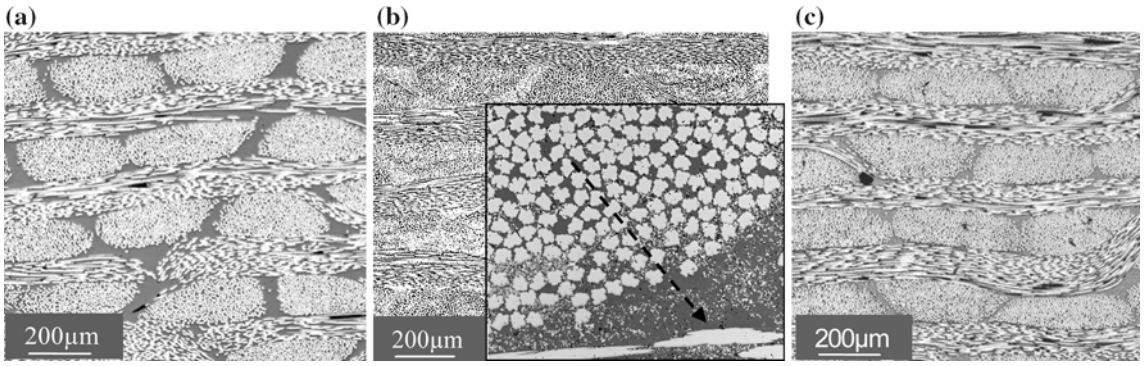

Fig. 9 Optical micrographs of **a** F/P, **b** F/P_f and **c** F_t/P_f composites after processing. Filler concentration gradient at bundles circumference is presented for one of the filler reinforced matrix composite on the microscopic enlargement (**b**)

When heat treated up to 600 °C, the F/P composite porosity mainly consists in two major populations: cracks with apparent entrance diameter of 0.1–10 µm and cracks above 100 µm width. The first population can be identified by optical microscopy (Fig. 7a) as *intra-bundle cracks* mainly directed in the plane of the 2D reinforcement. Intra-bundle cracks perpendicular to the plane also occur but are limited by transverse bundles. Matrix exhibit 10–20 µm width cracks perpendicularly to the reinforcement plane. It can be due to the resin carbonization with shrinkage that occur at this temperature, and cause high stress zones in the composites. The development of *delaminations* can be obtained, as the consequence of deflection of transversal cracks. The porosity of over 100 µm size is attributed to these large in-plane *inter-laminar cracks*. The matrix shrinkage is thus responsible for the *inter-bundle cracks*, but intra-bundle cracks initiation does not depend on the local matrix content. It could be due either to processing stress release started by composite thermal expansion or to the gas eliminated during the first step of the composite drying (330 °C) or resin decomposition (400–600 °C). At 800 °C, pre-existing cracks enlarge with a shift of population peak to higher diameter. In-plane inter-laminar cracks sizes grow over MIP-detected range as a consequence of matrix shrinkage. It allows releasing intra-bundle stress, and this effect combined with the matrix shrinkage within the bundles lead intra-bundle cracks to slightly close. The co-axial compression of bundles and the increase of matrix stiffness also lead the x–y bundle/bundle interfaces to fail and create a new population of inter-bundle cracks (10–50 µm) around the bundles in areas with lower amount of matrix. At 1,000 °C, no further shrinkage of the matrix happens, but cracks perpendicular to reinforcement direction extend within the bundles due to higher matrix stiffness (Fig. 10a).

The green F/P_f composite does not exhibit impregnation defects, but the filler dispersion in the matrix is not homogeneous. When the bundles are impregnated by the matrix, the filler cannot easily reach bundles core and get filtered by external fibres arrangement. It results in a high filler concentration layer around the bundle with a 30–40 µm thick gradient towards the inner bundle where no filler penetrates. When heat treated at 600 °C, the cracks distribution in this composite differs from the F/P composite. *Intra-bundle cracking* occurs but is not as systematic as in the F/P composite (Fig. 7b). On the other hand, *inter-bundle cracks* take place around each bundle in filler-rich zones. The fibre and filler concentration in these zones is high and may allow cracks to propagate because of the lack of matrix binder. Matrix rich-areas still cause through the thickness cracks in this case and inter-laminar large cracks extend by the inter-bundle cracks coalescence. At

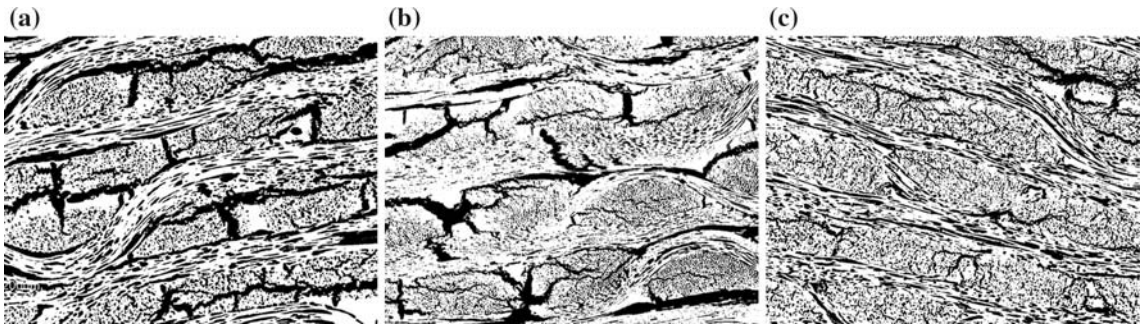

Fig. 10 Porosity network (*in black*) of the 1,000 °C heat treated composites **a** F/P, **b** F/P_f and **c** F_t/P_f characterized with optical microscopy

800 °C, shrinkage stresses seem to be relaxed through the extent of small-sized intra-bundle cracks in both z and (xy) directions, and *local fibre/matrix debonding* within the bundle. Up to 1,000 °C, the pre-existing cracks network grows and creates large inter-laminar and even inter-bundle cracks over 100 μm (Fig. 10b).

F_t/P_f at processing state does not show impregnation defect, but the same filler distribution is found as in the F/P_f green composite. When these composites are heat treated, the micrographs are drastically different from that of the two former. Resin-rich areas still produce through the thickness plane cracks of about 5 μm at 600 °C, but in a much lesser extent than for composites reinforced with F fibre (Fig. 7c). No crack over 10 μm is either seen or MIP detected. At the same time, a systematic fibre/matrix debonding (size around 1 μm) occurs and sometimes coalesces to produce 5–10 μm intra-bundles cracks. The fibre/matrix debonding pores further coalesce and intra-bundle cracks grow in all directions until 800 °C, and thus cause a peak shift on MIP curves. At 1,000 °C, pre-existing cracks and debonding network has extended, and a few major cracks (still under 500 μm) appears as the result of intra-bundle cracks growth (Fig. 10). At this temperature, neither inter-laminar cracks nor delamination phenomena have been seen, and the homogeneity of the F_t/P_f composite appears to be better than in the other two.

In the present study, the F/P porosity and cracks distribution are close in pattern and extent to those reported in former studies. Gao et al. [11] described the different inter-layer, inter-bundle and intra-bundle cracks in a cellulose-based carbon fibre eight-harness satin-weave impregnated with phenolic resin and pyrolysed up to 1,000 °C. The proposed classification of cracks can also be applied to F/P composite, and the porosity approximated by image analysis is in the same range of value (21.7%) as in the present case. More regular transverse cracks can be recorded with lower heating rate and plain-woven reinforcement as it was reported by Tzeng et al. [13].

A porosity emergence history is proposed taking into account microscopic recordings, quantitative porosity diameter and volume analyses performed on these materials.

The initial intra-bundle cracking created by gas evolution at 400 °C does not further extend once the bundle stress state has been relaxed. This relaxation may come from inter-laminar (F/P) or inter-bundle (F/P_f) crack propagation. In F/P, it causes smaller intra-bundle cracks to slightly close at 800 °C. After the bundle stress relaxation in F/P_f, the local stresses due to matrix shrinkage restrained by the linked fibres result in intra-bundles f/m debonding.

In F_t reinforced material, the initial fibre/matrix generalized debonding promotes a development of porosity network at microscopic scale during pyrolysis. Existence of such cracks network formed after interconnection between f/m debonding cracks allows relaxing enough stress and prevents the development of transversal cracking.

These results are in accordance with the study published by Schulte-Fischedick et al. [12].

Mechanical properties

The inter-laminar shear strength data as determined from the DNC test are reported in Table 4. This test has been reported to supply data comparable to other techniques [18] and it can be performed on composites with matrix at polymer and carbonized stage.

The test reproducibility is acceptable, even when samples do not fail in a perfect inter-laminar plane. The composites ILSS drop as the carbonization occurs. Failure occurs in inter-laminar plane for all kind of samples. ILSS values of carbonized composites remain low until 1,000 °C. Even if the addition of the filler modifies the development of cracks during the composite carbonization, no noticeable influence of these modifications could be noted on the 2D composite ILSS evaluation. The ILSS values for 1,000 °C carbonized composite are low when compared to published results for C/C (5–20 MPa) [3], although they remain of the same order as the 75 vol.% satin woven lamina materials tested with a DNC test by Li et al. [18] (ILSS: 7.80 ± 1.01). Here, the reinforcement geometry creates matrix rich domains in the composites, causing high local stresses and cracks that propagate within bundles or at inter-laminar interfaces.

The value of as cured F_t/P_f ILSS is lower than that of the two other materials. The lower fibre/matrix interfacial bond can possibly explain such a result. At higher temperature, the ILSS slightly increases. Because of the initial characteristic in the fibre/polymer matrix bonding, the matrix of the F_t/P_f obtained at 1,000 °C reveals cracks with noticeable differences in size and shape when compared to the F/P and F/P_f materials. This gives rise to a more homogeneous distribution of porosity together with less opened inter-laminar cracks. A better inter-laminar stress transfer can be responsible for this behaviour, due to (i) a less degraded inter-bundle linking and (ii) an increase of the intrinsic mechanical properties of this pyrolysed matrix.

Table 4 ILSS of heat treated composites (MPa)

Material	ILSS (MPa) F/P	F/P_f	F_t/P_f
As-cured	41.8 ± 0.9	36.1 ± 4.2	26.6 ± 1.0
600 °C	2.2 ± 0.3	3.1 ± 3.1	2.9 ± 0.3
800 °C	2.0 ± 0.7	1.9 ± 0.5	3.6 ± 0.9
1,000 °C	2.0 ± 0.5	2.3 ± 0.3	4.6 ± 0.9

Conclusion

First, as expected porosity and microstructure investigations of F/P, F/P_f, F_t/P_f composites at different stages of pyrolysis show the influence of interfacial bond on the characteristics of the materials. The F_t/P_f composite is the one showing the lower initial fibre/matrix bonding. All internal stresses generated during the composite pyrolysis are found to be released by fibre/matrix debonding and intra-bundle micro-cracking until 1,000 °C. Filler-rich matrix interfaces rarely fail, suggesting that the fibre/matrix interface is weaker than the filler/matrix one. Little amount of large cracks and no delamination have been observed for F_t/P_f C/C. The porosity at 1,000 °C occupies the same volume as in the two others composites, but distributed differently. It consists here in low diameter debondings and crackings (<10 μm) while untreated fibre reinforced composites exhibit mainly large cracks (>100 μm).

Second, it appears that the microstructural evolutions of the composite F_t/P_f are driven by the consequences of fibre/matrix low interfacial bonding. Others usually predominating parameters as 2D-satin reinforcement geometry, or bundles ability to exhaust carbonization gas have in this case minor effects. The cracks distribution is found to depend on filler repartition as well as filler/matrix bonding for the F/P_f composite, while it mainly depends on fibre/matrix interfacial strength for the F_t/P_f composite. Inter-laminar shear strength drops when resin pyrolysis initiates and remains low for the F/P and F/P_f materials. This property is not influenced by the presence of filler. There results suggest that the composite shear behaviour is ruled by fibre/matrix adhesion. Evolutions of ILSS values obtained at the final stage of pyrolysis confirm such an hypothesis.

Acknowledgements The authors are grateful to CNRS, CEA and Snecma Propulsion Solide (SPS) (SAFRAN- group) for the support in this work. They wish to thank G. Savignat from CEA for valuable discussions and for help with the mechanical test.

References

1. Trick KA, Saliba TE (1995) Carbon 33(11):1509
2. Wang CJ (1996) Reinforc Plast Compos 15:1011
3. Fitzer E, Manocha LM (1998) In: Carbon reinforcements and carbon/carbon composites. Berlin, Springer ed
4. Fukuyama K, Nishizawa T, Nishikawa K (2001) Carbon 39:2017
5. Lüdenbach G, Peters PWM, Ekenhorst D, Müller BR (1998) J Eur Cer Soc 11:1531
6. Ko TH, Kuo W-S, Chang Y-H (2000) Polym Compos 21(5):745
7. Rellick GS, Chang DJ, Zaldivar RJ (1992) J Mater Res 7:2798
8. Dhakate SR, Bahl P, Sahare PD (2000) J Mater Sci Lett 19:1959
9. Fitzer E, Geigl K-H, Manocha LM (1978). In: Proceedings of 5th London international carbon conference, p 405
10. Appleyard SP, Rand B (2002) Carbon 4:817
11. Gao F, Patrick JW, Walker A (1993) Carbon 31:103
12. Schulte-Fischedick J, Seiz S, Lützenburger N, Wanner A, Voggenreiter H (2007) Compos A 38:2171
13. Tzeng SS, Chr YG (2002) Mater Chem Phys 73:162
14. Lüdenbach G (1997) Düsseldorf, Fortschr. Ber. VDI, Reihe 5, Nr. 490, VDI-Verlag, D82, Diss, Dr.-Ing. RWTH Aachen
15. Wang S, Adanur S, Jang BZ (1997) Compos B 28(B):215
16. Savage G (1993) In: Carbon–carbon composites. Chapman & Hall, London
17. Baudry P, Pailler R, Dourges MA, Labrugère C (2004) Proceedings of 11th European conference on composite materials (ECCM 11)
18. Li M, Matsuyama R, Sakai M (1999) Carbon 3:1749
19. Sullivan RM, Stockes EH (1997) Mech Mater 26:197
20. Diamond S (2000) Cem Concr Res 30:1517
21. De With G, Glass HJ (1997) J Eur Cer Soc 17:753
22. Bacos M-P, Dorvaux J-M, Lavigne O, Renollet Y (2000) Carbon 38:77